IEEE Access
Multidisciplinary : Rapid Review : Open Access Journal

Received 12 April 2024, accepted 30 April 2024, date of publication 6 May 2024, date of current version 14 May 2024.

Digital Object Identifier 10.1109/ACCESS.2024.3397306

RESEARCH ARTICLE

Holographic Reconfigurable Intelligent Surface-Aided Downlink NOMA IoT Networks in Short-Packet Communication

DINH-TUNG VO[1], TAN N. NGUYEN[2], (Member, IEEE), ANH-TU LE[3,4], (Member, IEEE), VAN-DUC PHAN[5], AND MIROSLAV VOZNAK[3], (Senior Member, IEEE)

[1]HUTECH Institute of Engineering, HUTECH University, Ho Chi Minh City 70000, Vietnam
[2]Communication and Signal Processing Research Group, Faculty of Electrical and Electronics Engineering, Ton Duc Thang University, Ho Chi Minh City 70000, Vietnam
[3]Faculty of Electrical Engineering and Computer Science, VSB—Technical University of Ostrava, 708 00 Ostrava, Czech Republic
[4]Science and Technology Application for Sustainable Development Research Group, Ho Chi Minh City University of Transport, Ho Chi Minh City 700000, Vietnam
[5]Faculty of Automotive Engineering, School of Technology, Van Lang University, Ho Chi Minh City 70000, Vietnam

Corresponding author: Tan N. Nguyen (nguyennhattan@tdtu.edu.vn)

This work was supported in part by European Union within the REFRESH Project—Research Excellence For Region Sustainability and High-Tech Industries of European Just Transition Fund under Grant CZ.10.03.01/00/22_003/0000048; and in part by the Ministry of Education, Youth and Sports of the Czech Republic (MEYS CZ) conducted by VSB—Technical University of Ostrava through the SGS Project SP 7/2023.

ABSTRACT Non-orthogonal multiple access (NOMA) technology is projected to significantly increase the spectrum efficiency of the fifth-generation and subsequent wireless networks. Holographic reconfigurable Intelligent surfaces (HRISs) are a revolutionary technology that can deliver excellent spectral and energy efficiency at a cheap cost in wireless networks. In this letter, we investigate the short-packet communication (SPC) with the NOMA-based HRIS system with the internet of things (IoT). A base station (BS) communicates with two NOMA users by using HRIS in the proposed system to enhance spectral efficiency. Furthermore, we derived the exact closed-form expression of the average block error rate (BLER) for two NOMA users. To get more insight into the proposed system, the asymptotic BLER analysis was also carried out at high signal-to-noise ratio regime. The numerical results validate the current analysis and show that the presented NOMA strategy exceeds orthogonal multiple access-based approaches in terms of BLER and throughput.

INDEX TERMS Holographic reconfigurable intelligent surfaces, NOMA, short-packet communication, IoT, BLER.

I. INTRODUCTION

IoTs have allowed technologies for smart homes, smart cities, IoVs, smart industry, and space information networks, as well as plentiful device connections and sensors with many uses [1], [2], [3]. Massively networked smart devices pose difficult difficulties for the future of IoT B5G and mMTC [4]. As a consequence, the increased QoS demand for the 5G and future 6G communication networks has resulted in a shortage of resources (i.e., time slots, frequencies, and bandwidth) [5]. RIS has been deemed essential technology in many communication systems, including wireless sensor networks, and cellular networks, in order to support the connectivity of mMTC with varying QoS requirements and provide notable improvements in SE and EE [6], [7], [8]. Even so, RIS still faces some important limitations. Specifically, since RIS lacks signal processing capabilities, it cannot conduct channel estimation or beam tracking. Furthermore, RIS is

The associate editor coordinating the review of this manuscript and approving it for publication was Bilal Khawaja.

limited by the transmission bandwidth and hence the data rate is limited [6]. Therefore, HRIS was recently presented to surpass the aforementioned limitations [9], [10]. HRIS is compatible with all of the features offered by traditional RIS. In particular, HRISs are compatible with all of the features offered by traditional RIS. In particular, compared to conventional RIS, HRIS is able to support channel estimation and act like continuous surfaces for larger amounts of bandwidth [10], [11].

The technology known as URLLC has gained significant importance for next-generation networks, including 5G and 6G [12]. This is especially because URLLC can meet the high requirements of IoT applications, which demand ultralow latency ($\leqslant$ 1 ms) and high reliability (99.99%) [13], [14]. For low-latency systems, traditional analytical techniques based on Shannon capacity are no longer appropriate [15]. To lower physical-layer transmission latency for URLLCs, a novel transmission technique called SPC using FBL codes has been developed [16]. BLER, a recently developed statistic that has been extensively researched, is used to assess the effectiveness of SPC systems [17], [18], [19].

NOMA which enables multiple users to transmit data in the same resource block through different power allocations [20], [21], [22], has emerged as a viable strategy in recent years for enhancing the SE, reliability, and latency in future wireless communications [23]. SC and SIC are two techniques used by NOMA technology to service numerous users on the same time-frequency resource block [24]. By boosting system throughput through the simultaneous transmission of several signals on the same resource block, it makes large-scale IoT link communication possible [25].

Applying RIS technology to the NOMA system is strongly recommended as it offers a novel way to improve the performance of NOMA systems through the reconstruction of the wireless environment [26]. To enhance RIS-assisted NOMA systems' performance, two different phase shift designs have been studied [27]. Taking into account both ideal and non-ideal scenarios, a novel technique is provided to determine the maximum total rate of all users based on reflection amplitude and phase shift [28]. The study [29] investigated how well NOMA cellular networks use spectrum when utilizing RIS to provide coordinated multipoint broadcasts. References [30] and [31] examines a RIS-assisted two-users NOMA network's energy efficiency, outage probability, and coverage probability. In order to optimize user service in each orthogonal spatial direction while taking hardware limitations into account, the authors also suggest a RIS-NOMA architecture [32]. The authors in [33] study how the ergodic rate and outage probability are affected by faulty consecutive interference cancellation. To bridge the gap between RIS-assisted NOMA and user-relaying cooperation, the study recommends that a RIS-assisted cooperative-NOMA network should be investigated.

Based on the benefits obtained from the usage of RIS and NOMA, researchers are in the early stages of researching the combination of URLLC and RIS (URIS). The authors of [34] investigated the effect of phase errors and hardware impairments on the performance of URIS systems, whereas the authors of [35] studied the system with and without perfect CSI. In [36], an unmanned aerial vehicle-integrated UIRS system was developed to transport brief URLLC instruction packets between terrestrial IoT devices. In [37], the authors introduced a fountain-coded technique for cross-layer systems and improved PA coefficient to reduce transmission delay. The author in [38] derived the closed-form expression BLER under perfect and imperfect SIC with two case random and optimal phase shifts.

Most works only study the performance of RIS-NOMA [26], [27], [28], [29], [30], [31], [32], [33], [39], [40], HRIS-NOMA [41], [42], or "RIS-NOMA-integrated URLLC systems" [34], [35], [36], [37], [38]. However, the implementation of URLLC in HRIS-based NOMA systems has not been fully explored. Based on the above motivation and our knowledge to fill the existing gaps in the literature, this work focuses on the system performance by analyzing BLER. Table 1 summarizes the comparative novelty of our article with the existing studies. Specifically, our main contributions are summarized as follows:

- We proposed the HRIS-aided downlink NOMA IoT network in SPC.
- The closed-form BLER for the HRIS-aided NOMA IoT network is derived. Furthermore, to get more insight into the proposed system, the asymptotic BLER and throughput are also expressed.
- Monte Carlo simulation investigates the link between the proposed system's primary parameters and BLER and throughput and gives important insights into the influence of the main parameters on the BLER of the NOMA IoT system.

The organization of the paper is as follows. Section II presents the system model of the proposed HRIS-assisted NOMA system. The analysis of BLER is developed in Section III. The numerical results are provided in Section IV. Section V concludes this paper. The abbreviations and acronyms are presented in Table 2.

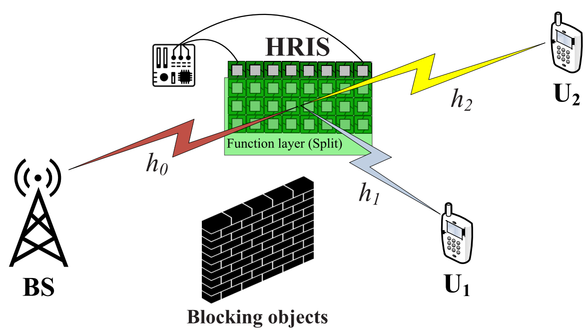

FIGURE 1. HRIS-assisted NOMA system.

TABLE 1. Comparison between the novelty of our work and previous papers.

Ref./Prop.	HRIS	Sorted channel	NOMA	SPC	Asymptotic	Throughput
[43]	X	X	✓	X	X	X
[44]	X	X	✓	✓	✓	✓
[45]	X	X	✓	✓	✓	X
[46]	X	X	✓	X	✓	X
[47]	X	X	✓	X	X	X
[48]	✓	X	X	X	X	X
[49]	✓	X	X	X	X	X
[50]	✓	X	X	X	X	X
Our study	✓	✓	✓	✓	✓	✓

TABLE 2. Abbreviations and Acronyms.

Acronym	Definition
6G	Six-generation
AWGN	Additive white Gaussian noise
B5G	Beyond 5G
BLER	Block error rat
BS	Base station
CSI	Channel state information
CDF	Cumulative distribution function
EE	Energy efficiency
FBL	Finite blocklength
HRISs	Holographic reconfigurable intelligent surfaces
IoT	Internet of thing
IoVs	Internet of vehicles
mMTC	Massive machine- type communication
NOMA	Non-orthogonal multiple access
OMA	Orthogonal multiple access
PDF	Probability density function
PA	Power allocation
QoS	Quality-of-service
RIS	Reconfigurable intelligent surface
SPC	Short-packet communication
SE	Spectral efficiency
SIC	Successive interference cancellation
SC	Superimposed coding
SINR	Signal-to-interference-plus-noise ratio
SNR	Signal-to-noise ratio
URLLC	Ultrareliable and low-latency communication

II. SYSTEM MODEL

We consider a downlink situation in a wireless system with HRIS assistance, as shown in Fig. 1. For example, BS uses a single HRIS to interact with two end-nodes, i.e., user equipment near user (U_1) and far user (U_2). The BS-HRIS, HRIS-U_1 and HRIS-U_2 connections are LoS, and it is assumed that both the BS and the two users have a single antenna, that perfect CSI can be obtained, and that a blocking object preventing direct transmission between the two users can be formed. Additionally, we assume that both the HRIS and UEs as well as the BS and HRIS have highly directed connections.

Let P_S denote the BS transmit power, x_1 and x_2 are the intended signals for the U_1 and U_2, respectively, which satisfies $\mathbb{E}\left\{|x_1|^2\right\} = \mathbb{E}\left\{|x_2|^2\right\} = 1$, where $\mathbb{E}\{.\}$ is the expectation operator. The BS transmits a composite signal, which can be expressed as

$$x = \sqrt{b_1 P_S} x_1 + \sqrt{b_2 P_S} x_2, \tag{1}$$

where b_1 and b_2 denote the power allocation coefficients with $b_1 < b_2$ and $b_1 + b_2 = 1$ [50], [51], [52].

By assuming that the HRIS's meta-atoms are highly linked, selecting the beam split functionality, and employing NOMA, the received signal at U_1 and U_2 may be produced as

$$q_i = \mathcal{A}_i x + w_i, i \in \{1, 2\}, \tag{2}$$

where $w_i \sim \mathcal{CN}\left(0, \sigma_i^2\right)$ denotes AWGB with mean zero and variance σ_i^2. Moreover, [9], [53],

$$\mathcal{A}_1 = h_0 h_1, \tag{3a}$$
$$\mathcal{A}_2 = h_0 h_2, \tag{3b}$$

where the complex channel coefficients of BS-HRIS, HRIS-U_1, and HRIS-U_2 connections are indicated by h_0, h_1 and h_2, respectively. The network's wireless connections are believed to be independent non-selective block Rayleigh fading. The distances for the BS-HRIS, HRIS-U_1, and HRIS-U_2 links are denoted as d_0, d_1 and d_2 respectively. α represents the path loss coefficient

Applying (1) and (2) yields the following

$$q_1 = \frac{\mathcal{A}_1}{\sqrt{d_0^\alpha d_1^\alpha}} \left(\sqrt{b_1 P_S} x_1 + \sqrt{b_2 P_S} x_2\right) + w_1, \tag{4a}$$
$$q_2 = \frac{\mathcal{A}_2}{\sqrt{d_0^\alpha d_2^\alpha}} \left(\sqrt{b_1 P_S} x_1 + \sqrt{b_2 P_S} x_2\right) + w_2, \tag{4b}$$

Without loss of generality, we assumed that the channel gains of HRIS-U_1 and HRIS-U_2 are ordered as $|h_2|^2 < |h_1|^2$; therefore, $|\mathcal{A}_2|^2 < |\mathcal{A}_1|^2$ and, according to the NOMA principle, $b_2 > b_1$. As a result, U_2 directly decodes x_2, considering x_1's interference as noise; consequently, the instantaneous signal-to-interference-plus-noise ratio (SINR) may be represented as

$$\gamma_{U_2}^{x_2} = \frac{P_S b_2 |\mathcal{A}_2|^2}{P_S b_1 |\mathcal{A}_2|^2 + d_0^\alpha d_2^\alpha \sigma_2^2} = \frac{\rho_S b_2 |\mathcal{A}_2|^2}{\rho_S b_1 |\mathcal{A}_2|^2 + d_0^\alpha d_2^\alpha}, \quad (5)$$

We assume that $\rho_S = \frac{P_S}{\sigma_1^2} = \frac{P_S}{\sigma_2^2}$ represents the average transmit SNR. In contrast, U_1 decodes x_2 first before using SIC to decode x_1. Consequently, it is possible to write the instantaneous SINR for decoding x_2 at U_1 as

$$\gamma_{U_1}^{x_2} = \frac{\rho_S b_2 |\mathcal{A}_1|^2}{\rho_S b_1 |\mathcal{A}_1|^2 + d_0^\alpha d_1^\alpha}. \quad (6)$$

The SNR for decoding x_1 in U_1 after SIC may be found as

$$\gamma_{U_1}^{x_1} = \frac{\rho_S b_1 |\mathcal{A}_1|^2}{d_0^\alpha d_1^\alpha}. \quad (7)$$

III. ANALYSIS OF BLER IN SHORT PACKET COMMUNICATION

In this section, we will begin by providing the channel statistics and some preliminary information about SPC. Following that, we will derive closed-form expressions for the average BLER for both far and near users.

A. CHANNEL STATISTICS

The lemmas that follow each return the statistical characterization of $|h_0|^2$, $|h_1|^2$, and $|h_2|^2$.

The PDF and CDF of $|h_0|^2$ can be expressed as [54]

$$f_{|h_0|^2}(x) = \frac{1}{\lambda_{h_0}} e^{-\frac{x}{\lambda_{h_0}}}, x > 0, \quad (8a)$$

$$F_{|h_0|^2}(x) = 1 - e^{-\frac{x}{\lambda_{h_0}}}, x > 0, \quad (8b)$$

where $\lambda_{h_0} = E\left\{|h_0|^2\right\}$ is the mean of $|h_0|^2$.

Lemma 1: In this Lemma, the CDF of $|\mathcal{A}_2|^2$ can be derived as

$$F_{|\mathcal{A}_2|^2}(z) = 1 - \sqrt{4\varphi z} K_1\left(\sqrt{4\varphi z}\right). \quad (9)$$

where K_1 denotes the first-order modified Bessel function of the second kind [55].

Proof: To be concise, the proof of Lemma 1 is presented in Appendix A. ■

Lemma 2: The CDF of $|\mathcal{A}_1|^2$ can be expressed as

$$F_{|\mathcal{A}_1|^2}(z) = 1 - \sqrt{\frac{4z}{\lambda_{h_0}\lambda_{\bar{h}_2}}x} K_1\left(\sqrt{\frac{4z}{\lambda_{h_0}\lambda_{\bar{h}_2}}x}\right) - \sqrt{\frac{4z}{\lambda_{h_0}\lambda_{\bar{h}_1}}x} K_1\left(\sqrt{\frac{4z}{\lambda_{h_0}\lambda_{\bar{h}_1}}x}\right) + \sqrt{4\varphi z x} K_1\left(\sqrt{4\varphi z x}\right). \quad (10)$$

Proof: The proof of Lemma 2 is shown in Appendix B. ■

B. PRELIMINARIES

SPC is gaining popularity and becoming an essential trend in IoT. However, traditional Shannon theory, which was developed under the assumption of unlimited blocklength, is no longer directly applicable in the context of SPC. In response to this challenge, Polyanskiy and his colleagues, as documented in [16], pioneered the derivation of the highest achievable rate for a given blocklength $\mathcal{L}$, SINR γ, and BLER ε, as further discussed in [56].

$$\mathcal{R} = \log_2(1+\gamma) - \frac{\mathcal{Q}^{-1}(\varepsilon)}{\ln 2}\sqrt{\frac{\mathcal{V}(\gamma)}{\mathcal{L}}}, \quad (11)$$

where $\mathcal{V}(x) = 1 - (1+x)^{-2}$, $\mathcal{Q}^{-1}(x) = \frac{1}{2\pi}\int_x^\infty e^{-\frac{t^2}{2}}dt$ is the inverse of the Gaussian Q-function. From (26), we can compute the instantaneous BLER of decoding the message of U_i, $i \in \{1, 2\}$ as follows:

$$\varepsilon_K \approx \mathcal{Q}\left(\ln 2 \frac{\log_2(1+\gamma_K) - \tilde{R}_K}{\sqrt{\mathcal{V}(\gamma_K)/\mathcal{L}_K}}\right), K \in \{U_1, U_2\} \quad (12)$$

Here, we have $\tilde{R}_K = \eta_K/\mathcal{L}_K$, where η_K represents the number of information bits and $\mathcal{L}_K$ represents the blocklength for user K. For the sake of simplifying subsequent analysis, $\mathcal{L}_K$ can be approximated in a close and more manageable manner as:

$$\varepsilon_K = \begin{cases} 1 & \gamma_K \le \alpha_K \\ \frac{1}{2} - g_K\sqrt{\mathcal{L}_K}(\gamma_K - h_K) & \alpha_K < \gamma_K < \beta_K \\ 0 & \gamma_K \ge \beta_K \end{cases} \quad (13)$$

where $g_K = \frac{1}{\sqrt{2\pi\left(2^{2\tilde{R}_K}-1\right)}}$, $h_K = 2^{\tilde{R}_K}-1$, $\alpha_K = h_K - \frac{1}{2g_K\sqrt{\mathcal{L}_K}}$ and $\beta_K = h_K + \frac{1}{2g_K\sqrt{\mathcal{L}_K}}$.

From (28), the average BLER $\tilde{\varepsilon}_K \triangleq \mathbb{E}[\varepsilon_K]$ is given by

$$\tilde{\varepsilon}_K = \int_0^\infty \varepsilon_K f_{\gamma_K}(x)dx = g_K\sqrt{\mathcal{L}_K}\int_{\beta_K}^{\alpha_K} F_{\gamma_K}(x)dx. \quad (14)$$

C. AVERAGE BLER ANALYSIS OF NEAR USER

Proposition 1: The closed-form expression of the average BLER for U_1 is written as

$$\tilde{\varepsilon}_{U_1} = 1 - 4g_{U_1}\sqrt{\mathcal{L}_{U_1}} \times \left[\frac{1}{\upsilon_2}\lambda\left(\frac{4}{\upsilon_2\beta_{U_1}}, \frac{4}{\upsilon_2\alpha_{U_1}}\right) + \frac{1}{\upsilon_1}\lambda\left(\frac{4}{\upsilon_1\beta_{U_1}}, \frac{4}{\upsilon_1\alpha_{U_1}}\right) - \frac{1}{\upsilon_3}\lambda\left(\frac{4}{\upsilon_3\beta_{U_1}}, \frac{4}{\upsilon_3\alpha_{U_1}}\right)\right], \quad (15)$$

where $\lambda(x, y)$, as shown at the bottom of the next page, and $\mathcal{H}_{p,q:u,v:e,f}^{m,n:s,t:i,j}(\cdot)$ represents the extended generalized bivariate Fox H-function (EGBFHF) in [57].

Proof: See Appendix C. ■

D. AVERAGE BLER ANALYSIS OF FAR USER

Proposition 2: The approximate closed-form expression of the average BLER for U_2 is provided as

$$\tilde{\varepsilon}_{U_2} \approx 1 - \frac{\pi g_{U_2}\sqrt{\mathcal{L}_{U_2}}\left(\beta_{U_2}-\alpha_{U_2}\right)}{2W} \times \sum_{w=1}^{W}\sqrt{1-\upsilon_w^2}\, G_{0,2}^{2,0}\left(\varphi\hat{\theta}_2\left(\chi_w\right)\middle|\begin{matrix}-\\1,0\end{matrix}\right), \tag{17}$$

where W is the number of integration points, $\upsilon_w = \cos\left(\frac{2w-1}{2W}\pi\right)$ and $\chi_w = \upsilon_w\left(\frac{\beta_{U_2}-\alpha_{U_2}}{2}\right)+\left(\frac{\alpha_{U_2}+\beta_{U_2}}{2}\right)$.

Proof: See Appendix D. ■

However, the extended generalized bivariate Fox H-function in (15) is hard to model and adds a significant amount of computational complexity. To get around this problem, we may use the midpoint approximation approach to get an estimate for $\tilde{\varepsilon}_{U_1}$ and $\tilde{\varepsilon}_{U_2}$ in the following equation. Given that there is not much of a difference between α_K and β_K, $K \in \{U_1, U_2\}$ in (46) and (54) [38], we can further simplify

$$\tilde{\varepsilon}_{U_1}^{App} = \sum_{o=1}^{O}\frac{1}{O}\Big[1-\sqrt{\upsilon_2\zeta_{1,o}}K_1\left(\sqrt{\upsilon_2\zeta_{1,o}}\right)-\sqrt{\upsilon_1\zeta_{1,o}} \times K_1\left(\sqrt{\upsilon_1\zeta_{1,o}}\right)+\sqrt{\upsilon_3\zeta_{1,o}}K_1\left(\sqrt{\upsilon_3\zeta_{1,o}}\right)\Big], \tag{18}$$

and

$$\tilde{\varepsilon}_{U_2}^{App} = \sum_{o=1}^{O}\frac{1}{O}\left[1-\sqrt{\frac{\phi\zeta_{2,o}}{b_2-b_1\zeta_{2,o}}}K_1\left(\sqrt{\frac{\phi\zeta_{2,o}}{b_2-b_1\zeta_{2,o}}}\right)\right], \tag{19}$$

where $\zeta_{1,o} = \alpha_{U_1}+(2o-1)\left(\beta_{U_1}-\alpha_{U_1}\right)/2O$, $\phi = \frac{4\varphi d_0^\alpha d_2^\alpha}{\rho_S}$, $\zeta_{2,o} = \alpha_{U_2}+(2o-1)\left(\beta_{U_2}-\alpha_{U_2}\right)/2O$ and O implies the complexity accuracy trade-off parameter.

E. AVERAGE ASYMPTOTIC BLER ANALYSIS

From (14), by utilizing the first-order Riemann integral approximation, $\tilde{\varepsilon}_{U_i}$, $i \in \{1, 2\}$ can be approximated as

$$\tilde{\varepsilon}_{U_i}^{Asym} \approx F_{\gamma_{U_i}^{x_i}}\left(h_{U_i}\right). \tag{20}$$

Based on (45) analytical finding, the average asymptotic BLER at U_1 at high SNR is given by

$$\tilde{\varepsilon}_{U_1}^{Asym} = -\frac{2\tilde{\theta}_1}{\lambda_{h_0}}\left[\frac{1}{\lambda_{\bar{h}_2}}\ln\left(\sqrt{\frac{\tilde{\theta}_1}{\lambda_{h_0}\lambda_{\bar{h}_2}}}\right)+\frac{1}{\lambda_{\bar{h}_1}} \times \ln\left(\sqrt{\frac{\tilde{\theta}_1}{\lambda_{h_0}\lambda_{\bar{h}_1}}}\right)-\lambda_{h_0}\varphi\ln\left(\sqrt{\tilde{\theta}_1\varphi}\right)\right], \tag{21}$$

where $\tilde{\theta}_1 = \frac{h_{U_1}d_0^\alpha d_1^\alpha}{\rho_S b_1}$.

Remark 1: From the average asymptotic BLER at U_1 in (21), it provides some useful insight as follows: *i*) the BLER at U_1 is improved when increasing the transmit SNR ρ_S, the power allocation b_1 and the average of channel λ_{h_0}, $\lambda_{\bar{h}_1}$ and $\lambda_{\bar{h}_1}$. *ii*) The diversity order of U_1 is one.

Proof: To make the computation easier, we use the series form of the Bessel function $K_n(x)$ to approximate the high SNR. $K_n(x)$ can be approximated when $n = 1$ as

$$K_1(x) \approx \frac{x}{2}\ln\left(\frac{x}{2}\right)+\frac{1}{x}. \tag{22}$$

It can be obtained (21) by putting (22) into (20), respectively. The proof is finished. ■

Similarly, we may get the asymptotic expression for user U_1. the average asymptotic BLER equation that correlates to the performance of user U_2 is provided by

$$\tilde{\varepsilon}_{U_2}^{Asym} = -2\tilde{\theta}_2\varphi\ln\left(\sqrt{\tilde{\theta}_2\varphi}\right), \tag{23}$$

where $\tilde{\theta}_2 = \frac{h_{U_2}d_0^\alpha d_2^\alpha}{\rho_S\left(b_2-b_1h_{U_2}\right)}$.

Remark 2: From the average asymptotic BLER at U_2 in (23), it provides some useful insight as follows: *i*) the BLER at U_2 is improved when increasing the transmit SNR ρ_S, the average of channel λ_{h_0}, $\lambda_{\bar{h}_1}$ and $\lambda_{\bar{h}_1}$. *ii*) The BLER at U_2 satisfy $b_2 - b_1h_{U_2} > 0$ otherwise The BLER at U_2 is one. *iii*) The diversity order of U_1 is also one.

F. SYSTEM THROUGHPUT ANALYSIS

In order to illustrate the benefits of the investigated system in terms of latency reduction over its orthogonal equivalent, we also offer performance measures throughput, focusing on the influence of the non-zero error probability on progressively decoding the signals at the users. More specifically, the metric to assess the efficiency of communication across the constant channel coding rate, $\bar{R}_{U_i}$, is the throughput in nats per channel usage (npcu). In mathematical terms, the throughput is determined by multiplying $\bar{R}_{U_i}$ by the packet that the user is repeatedly decoding e2e $\left(1-\tilde{\varepsilon}_{U_1}\right)$. Furthermore, the total throughput of the system is represented as [44]

$$\tau_{system} = \left(1-\tilde{\varepsilon}_{U_1}\right)\bar{R}_{U_1}+\left(1-\tilde{\varepsilon}_{U_2}\right)\bar{R}_{U_2}. \tag{24}$$

IV. NUMERICAL RESULTS

In this section, Monte Carlo simulations (labeled as "Sim.") are employed to validate the analytical computation, (labeled as "Ana."), approximation curves (labeled as "Appr."), and asymptotic results (labeled as "Asym."). These simulations are conducted using the settings outlined in Table 3. Additionally, the equivalent noise power at U_1 and U_2 was calculated as $\sigma_1^2 = \sigma_2^2 = N_0 + 10\log(BW) + NF$ [dBm] in [47] and the complexity accuracy trade-off parameter is set

$$\lambda(a,b) = \mathcal{H}_{2,0:1,1:1,1}^{0,2:1,0:0,1}\left(\begin{matrix}(-1;1,1);(0;1,1)\\-\end{matrix}\middle|\begin{matrix}(1,1)\\(0,1)\end{matrix}\middle|\begin{matrix}(1,1)\\(0,1)\end{matrix}\middle|a,b\right). \tag{16}$$

TABLE 3. Main parameters for our simulations.

Monte Carlo simulations	10^7 iterations
Power allocation factors	$b_1 = 0.2$ and $b_2 = 0.8$
Fading means	$\lambda_{h_0} = \lambda_{\bar{h}_1} = \lambda_{\bar{h}_2} = 1$
Bandwidth	$BW = 10$ [MHz]
Noise figure	$NF = 10$ [dBm]
Thermal noise power density	$N_0 = -174$ [dBm/Hz]
The distance from BS to HRIS	$d_0 = 60$ [m]
The distance from HRIS to U_1	$d_1 = 100$ [m]
The distance from HRIS to U_2	$d_2 = 150$ [m]
The path loss exponent	$\alpha = 2$
Number of information bits	$\eta_{U_1} = 150$ and $\eta_{U_2} = 100$
Blocklength	$\mathcal{L} = \mathcal{L}_{U_1} = \mathcal{L}_{U_2} = 200$

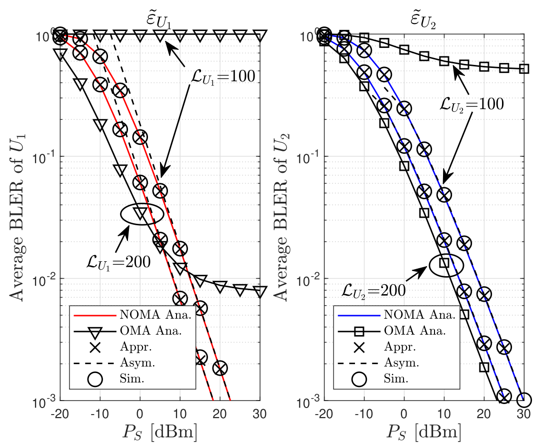

FIGURE 2. Average BLER versus P_S different $\mathcal{L}$.

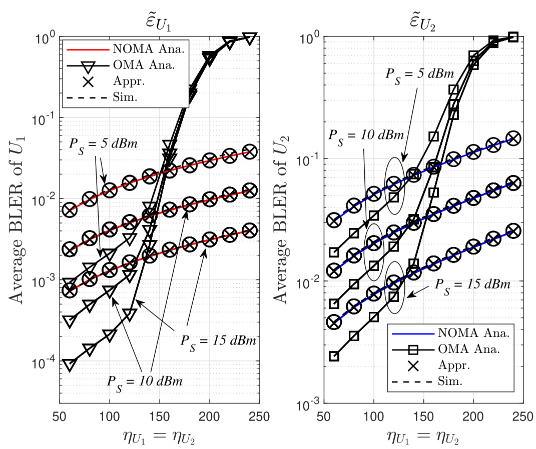

FIGURE 3. Average BLER versus η_{U_1} and η_{U_2} different P_S.

to $W = O = 100$ to ensure a close approximation. Notably, our code's technological innovation lies in the utilization of symbolic calculations within Matlab, which has enabled us to achieve highly accurate results. It should be noted that, in the case of OMA, the SINR criteria for successful decoding are specified as $\gamma_{thi}^{OMA} = 2^{2R_i} - 1, i \in \{1, 2\}$.

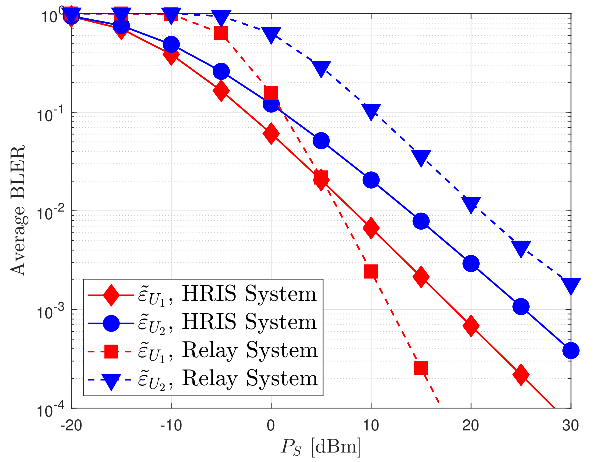

FIGURE 4. Comparison of average BLER versus P_S between HRIS/relay.

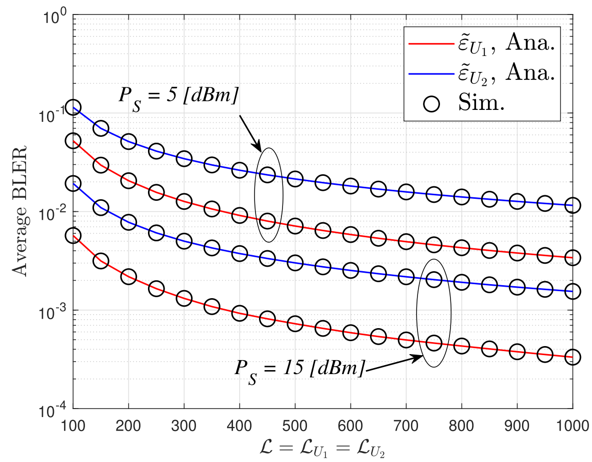

FIGURE 5. Average BLER versus blocklength ($\mathcal{L}$), with $\eta_{U_1} = 150$, $\eta_{U_2} = 100$ and $P_S = \{5, 15\}$ [dBm].

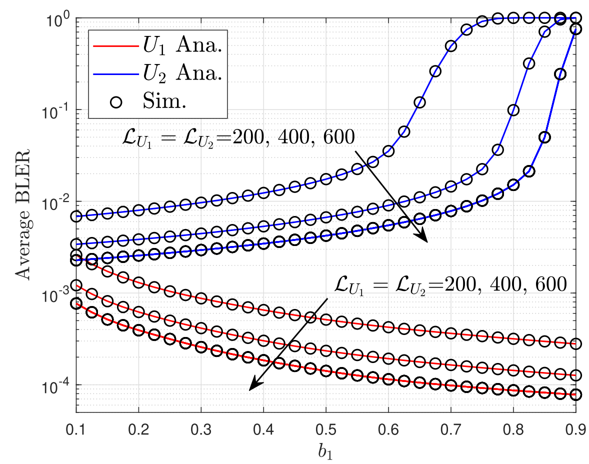

FIGURE 6. Average BLER versus b_1 different $\mathcal{L}$ with $P_S = 15$ dBm and $\eta_{U_1} = \eta_{U_2} = 100$.

Fig. 2 shows the BLER versus P_S[dBm] with varying the blocklength for two NOMA users. First, we can observe that the analytical points nearly match the simulation curves, confirming the derivations' correctness. Second, when P_S

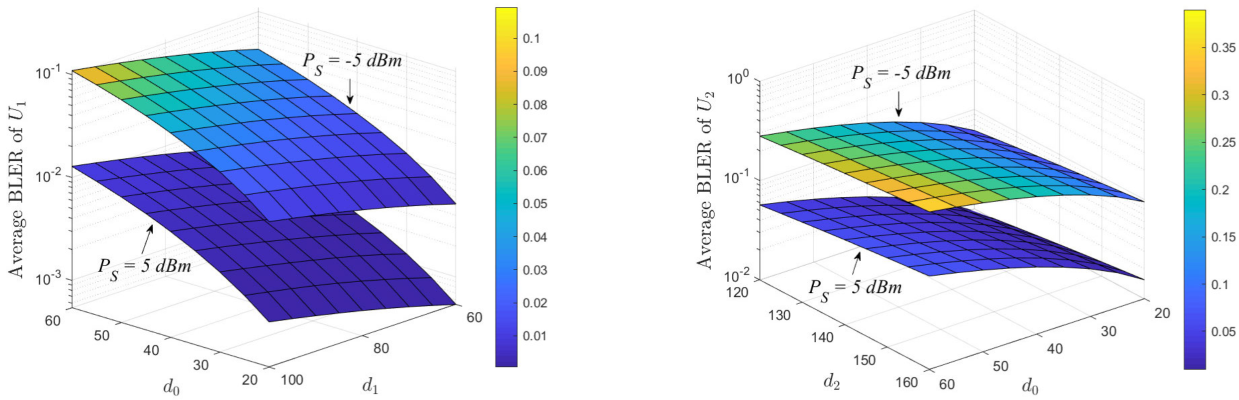

(a) Average BLER of U_1 versus d_0 and d_1 different P_S.

(b) Average BLER of U_2 versus d_0 and d_2 different P_S.

FIGURE 7. Average BLER of two users U_1 and U_2 with $\mathcal{L} = 200$ and $\eta_{U_1} = 100$.

grows, the BLER of both U_1 and U_2 reduces dramatically. This is because increasing P_S increases the SINR of both users, resulting in improved BLER performance. We can also see that when blocklength increases, BLER falls, demonstrating that short-packet transmission degrades reliability. Additionally, BLER NOMA performance of U_1 is always better than BLER OMA in the high P_S region. Furthermore, the BLER NOMA performance of U_2 is always better than BLER OMA when $\mathcal{L}_{U_2} = 100$, and worse than BLER OMA when $\mathcal{L}_{U_2} = 200$.

In Fig. 3, it plots the BLER of two users U_1 and U_2 versus the number of information bits. It can be observed that the BLER is increasing when the information bit is increasing for two users. The BLER performance of short information is better than that of the long information. In addition, the BLER OMA is better than NOMA in short information. When the information bit increases by 150, the BLER NOMA is always better than OMA and BLER OMA goes to 1. Fig. 6 plots the BLER versus the power allocation factor b_1 with different blocklength $\mathcal{L}$. First, we can observe that the BLER of U_1 drops when increasing b_1. However, the BLER of U_2 keeps growing when increasing b_1. It could be explained that increasing b_1 improves the power allocated to U_1, which improves the U_1's BLER. As a result, when increasing b_1 reduces the power provided to the U_2, which raises the BLER. Finally, Fig. 6 indicates that longer blocklength improved BLER performance for various b_1.

In Fig. 4, we compare the average BLER between the HRIS-aided system and the relay-aided System. The results show that the performance of the HRIS scheme is better than the relay scheme. The reason for this is that by suitably adjusting the phases of the reflecting element, the HRIS can improve the received SNR and improve the channel quality.

Fig. 5 plots the average BLER of two users versus the blocklength $\mathcal{L} = \mathcal{L}_{U_1} = \mathcal{L}_{U_1}$. As can be observed in Fig. 5, the average BLER of two users is improved when increasing the blocklength $\mathcal{L}$. In addition, the average BLER is decreased when the transmit power at BS is increased as in Fig. 2.

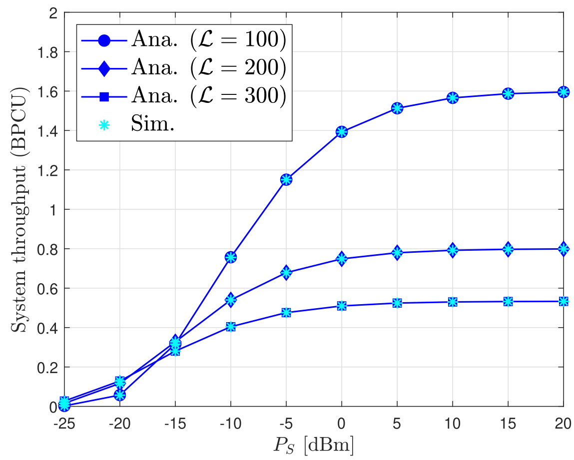

FIGURE 8. System throughput versus P_S different $\mathcal{L}$.

Fig 7 shows the BLER of U_1 and U_2 versus the distance and varying the power P_S. First, we can easily observe in Fig 7a and Fig 7b that when increasing the distance from BS to HRIS d_0, from HRIS to U_1 d_1, and from HRIS to U_2 d_2 the BLER is growing. This comes from the fact that when U_1 and U_2 are far from BS and RHIS, the SINR of U_1 and U_2 detects its own signal is difficult which means the SINR of two users will be dropping. On the other hand, the BLER performance will be improved when increasing the power at BS P_S, which comes from P_S growth leading to SNR increasing.

Fig. 8 depicts the throughput of the system versus P_S[dBm] and different the blocklength $\mathcal{L}$. As shown in Fig. 8, We can see that the throughput increases as the transmit power increases, indicating that increased transmit power also improves transmission efficiency. Because of the restricted packet length and quantity of information bits, increasing transmit power cannot indefinitely improve throughput. Additionally, decreasing the blocklength improves throughput performance since it is based on the relation $\bar{R}_{U_i} = \eta_{U_i}/\mathcal{L}_{U_i}$, where $\bar{R}_{U_i}$ falls as $\mathcal{L}_{U_i}$ gets longer and the throughput consequently declines continually.

V. CONCLUSION

In this paper, we study the SPC in HRIS-aided downlink NOMA IoT network, where HRIS supports transmitting the FBL packets from BS to two users. The performance of the proposed system in terms of BLER and throughput is investigated. The closed-form expression BLER and throughput are derived by adopting the approximate Chebyshev-Gauss quadrature and the EGBFHF, and verified by Monte Carlo simulations. In terms of BLER, the performance of the HRIS-NOMA system is compared to that of the HRIS-OMA system. According to the results, the HRIS-NOMA system outperforms the HRIS-OMA system. Furthermore, the result shows the effect of the power allocation factor on the performance of the proposed system, and the optimization approach will be left for future development. Finally, the packet length may be tuned to get the greatest ET of the proposed system.

APPENDIX A
PROOF OF LEMMA 1

Assuming that $|\bar{h}_1|$ and $|\bar{h}_2|$ are independent random variables with Rayleigh distribution parameters $\lambda_{\bar{h}_1}$ and $\lambda_{\bar{h}_2}$, respectively, and that $|\bar{h}_1|$ and $|\bar{h}_2|$ are sorted, the CDF of the ordered random variable $|h_2| = \min\left(|\bar{h}_1|, |\bar{h}_2|\right)$ may be computed as

$$F_{|h_2|}(y) = \Pr\left(|h_2| < y\right) = \Pr\left(\min\left(|\bar{h}_1|, |\bar{h}_2|\right) < y\right). \quad (25)$$

This may be rewritten as

$$F_{|h_2|}(y) = 1 - \left(1 - \Pr\left(|\bar{h}_1| < x\right)\right)\left(1 - \Pr\left(|\bar{h}_2| < x\right)\right). \quad (26)$$

It is noted that, we can rewrite (26) as

$$F_{|h_2|}(y) = F_{|\bar{h}_1|}(y) + F_{|\bar{h}_2|}(y) - F_{|\bar{h}_1|}(y)\, F_{|\bar{h}_2|}(y). \quad (27)$$

By taking into account that $|\bar{h}_1|$ and $|\bar{h}_2|$ follow Rayleigh distribution, (27) can be rewritten as

$$F_{|h_2|}(y) = \sum_{i=1}^{2}\left(1 - e^{-\frac{y^2}{\lambda_{\bar{h}_i}}}\right) - \prod_{j=1}^{2}\left(1 - e^{-\frac{y^2}{\lambda_{\bar{h}_j}}}\right). \quad (28)$$

where $\lambda_{\bar{h}_1} = \mathbb{E}\left\{|\bar{h}_1|^2\right\}$ and $\lambda_{\bar{h}_2} = \mathbb{E}\left\{|\bar{h}_2|^2\right\}$ are the mean of the corresponding unordered random variables $|\bar{h}_1|^2$ and $|\bar{h}_2|^2$, respectively. By setting $y = \sqrt{x}$, we have $F_{|h_2|^2}(x) = F_{|h_2|}\left(\sqrt{y}\right)$, the CDF of $|h_2|^2$ can be obtained as

$$F_{|h_2|^2}(x) = \sum_{i=1}^{2}\left(1 - e^{-\frac{x}{\lambda_{\bar{h}_i}}}\right) - \prod_{j=1}^{2}\left(1 - e^{-\frac{x}{\lambda_{\bar{h}_j}}}\right), \quad (29)$$

From (3b), the CDF of $F_{|\mathcal{A}_2|^2}(z)$ is calculated as

$$F_{|\mathcal{A}_2|^2}(z) = \Pr\left(|h_0|^2 |h_2|^2 < z\right). \quad (30)$$

Then, (30) is rewritten as follows

$$F_{|\mathcal{A}_2|^2}(z) = \Pr\left(|h_2|^2 < \frac{z}{|h_0|^2}\right) = \int_0^\infty f_{|h_0|^2}(x)\left[F_{|h_2|^2}\left(\frac{z}{x}\right)\right] dx. \quad (31)$$

Substituting (8a) and (29) into (31), $F_{|\mathcal{A}_2|^2}(z)$ can be obtained by

$$\begin{aligned} F_{|\mathcal{A}_2|^2}(z) &= \frac{1}{\lambda_{h_0}}\int_0^\infty e^{-\frac{x}{\lambda_{h_0}}}\left[\sum_{i=1}^{2}\left(1 - e^{-\frac{z}{x\lambda_{\bar{h}_i}}}\right)\right. \\ &\quad \left. - -\prod_{j=1}^{2}\left(1 - e^{-\frac{z}{x\lambda_{\bar{h}_i}}}\right)\right] dx \\ &= D_1(z) + D_2(z) - D_3(z), \end{aligned} \quad (32)$$

we have $D_1(z)$, $D_2(z)$ and $D_3(z)$ calculated as follows

$$D_1(z) = \frac{1}{\lambda_{h_0}}\int_0^\infty e^{-\frac{x}{\lambda_{h_0}}}\left(1 - e^{-\frac{z}{x\lambda_{\bar{h}_1}}}\right) dx, \quad (33a)$$

$$D_2(z) = \frac{1}{\lambda_{h_0}}\int_0^\infty e^{-\frac{x}{\lambda_{h_0}}}\left(1 - e^{-\frac{z}{x\lambda_{\bar{h}_2}}}\right) dx, \quad (33b)$$

$$D_3(z) = \frac{1}{\lambda_{h_0}}\int_0^\infty e^{-\frac{x}{\lambda_{h_0}}}\left(1 - e^{-\frac{z}{x\lambda_{\bar{h}_1}}}\right)\left(1 - e^{-\frac{z}{x\lambda_{\bar{h}_2}}}\right) dx. \quad (33c)$$

With the help of [55, Eq. (3.324.1)] and after some algebraic manipulations, the CDF of $F_{|\mathcal{A}_2|^2}(z)$ can be obtained by

$$F_{|\mathcal{A}_2|^2}(z) = 1 - \sqrt{4\varphi z}\, K_1\left(\sqrt{4\varphi z}\right). \quad (34)$$

The proof of Lemma 1 is completed.

APPENDIX B
PROOF OF LEMMA 2

Notice that $|h_1| = \max\left(|\bar{h}_1|, |\bar{h}_2|\right)$; thus, the CDF of $|h_1|$ can be obtained as

$$F_{|h_1|}(y) = \Pr\left(|h_1| < y\right) = \Pr\left(\max\left(|\bar{h}_1|, |\bar{h}_2|\right) < y\right). \quad (35)$$

By accounting for the independence of $|\bar{h}_1|$ and $|\bar{h}_2|$, $F_{|h_1|}(y)$ can be written as

$$F_{|h_1|}(y) = \Pr\left(|\bar{h}_1| < y\right)\Pr\left(|\bar{h}_2| < y\right) = F_{|\bar{h}_1|}(y)\, F_{|\bar{h}_2|}(y). \quad (36)$$

It is able to be expressed as

$$F_{|h_1|}(y) = \left(1 - e^{-\frac{y^2}{\lambda_{\bar{h}_1}}}\right)\left(1 - e^{-\frac{y^2}{\lambda_{\bar{h}_2}}}\right). \quad (37)$$

By setting $y=\sqrt{x}$, (37) returns as

$$F_{|h_1|^2}(x)=\prod_{j=1}^{2}\left(1-e^{-\frac{x}{\lambda_{\bar{h}_j}}}\right). \tag{38}$$

Next, the CDF of $F_{|\mathcal{A}_1|^2}(z)$ is calculated as follows

$$F_{|\mathcal{A}_1|^2}(z)=\Pr\left(|h_0|^2|h_1|^2<z\right). \tag{39}$$

It is noted that we can rewrite (39) as

$$\begin{aligned}F_{|\mathcal{A}_1|^2}(z)&=\Pr\left(|h_1|^2<\frac{z}{|h_0|^2}\right)\\&=\int_0^\infty f_{|h_0|^2}(x)\left[F_{|h_1|^2}\left(\frac{z}{x}\right)\right]dx.\end{aligned} \tag{40}$$

Substituting (38) and (8a) into (40), the CDF of $F_{|\mathcal{A}_1|^2}(z)$ is written as

$$\begin{aligned}F_{|\mathcal{A}_1|^2}(z)&=\frac{1}{\lambda_{h_0}}\int_0^\infty e^{-\frac{x}{\lambda_{h_0}}}\prod_{j=1}^{2}\left(1-e^{-\frac{z}{x}}\right)dx\\&=\frac{1}{\lambda_{h_0}}\int_0^\infty e^{-\frac{x}{\lambda_{h_0}}}-\frac{1}{\lambda_{h_0}}\int_0^\infty e^{-\frac{x}{\lambda_{h_0}}}\\&\quad\times\left(e^{-\frac{z}{x\lambda_{\bar{h}_2}}}-e^{-\frac{z}{x\lambda_{\bar{h}_1}}}+e^{-\frac{z}{x}\left(\frac{1}{\lambda_{\bar{h}_1}}+\frac{1}{\lambda_{\bar{h}_2}}\right)}\right)dx\\&=1-C_1(z)-C_2(z)+C_3(z),\end{aligned} \tag{41}$$

in which

$$C_1(z)=\frac{1}{\lambda_{h_0}}\int_0^\infty e^{-\frac{x}{\lambda_{h_0}}-\frac{z}{x\lambda_{\bar{h}_2}}}dx, \tag{42a}$$

$$C_2(z)=\frac{1}{\lambda_{h_0}}\int_0^\infty e^{-\frac{x}{\lambda_{h_0}}-\frac{z}{x\lambda_{\bar{h}_1}}}dx, \tag{42b}$$

$$C_3(z)=\frac{1}{\lambda_{h_0}}\int_0^\infty e^{-\frac{x}{\lambda_{h_0}}-\frac{z}{x}\left(\frac{1}{\lambda_{\bar{h}_1}}+\frac{1}{\lambda_{\bar{h}_2}}\right)}dx. \tag{42c}$$

Applying [55, Eq. (3.324.1)] and some polynomial expansion manipulations, C_1, C_2 and C_3 can be calculated as

$$C_1(z)=\sqrt{\frac{4z}{\lambda_{h_0}\lambda_{\bar{h}_2}}}xK_1\left(\sqrt{\frac{4z}{\lambda_{h_0}\lambda_{\bar{h}_2}}x}\right), \tag{43a}$$

$$C_2(z)=\sqrt{\frac{4z}{\lambda_{h_0}\lambda_{\bar{h}_1}}}xK_1\left(\sqrt{\frac{4z}{\lambda_{h_0}\lambda_{\bar{h}_1}}x}\right), \tag{43b}$$

$$C_3(z)=\sqrt{4\varphi zx}K_1\left(\sqrt{4\varphi zx}\right), \tag{43c}$$

where $\varphi=\frac{1}{\lambda_{h_0}}\left(\frac{1}{\lambda_{\bar{h}_1}}+\frac{1}{\lambda_{\bar{h}_2}}\right)$.

Substituting (43c), (43b) and (43a) into (41), the CDF of $|\mathcal{A}_1|^2$, is given by

$$\begin{aligned}F_{|\mathcal{A}_1|^2}(z)=1&-\sqrt{\frac{4z}{\lambda_{h_0}\lambda_{\bar{h}_2}}}xK_1\left(\sqrt{\frac{4z}{\lambda_{h_0}\lambda_{\bar{h}_2}}x}\right)\\&-\sqrt{\frac{4z}{\lambda_{h_0}\lambda_{\bar{h}_1}}}xK_1\left(\sqrt{\frac{4z}{\lambda_{h_0}\lambda_{\bar{h}_1}}x}\right)\\&+\sqrt{4\varphi zx}K_1\left(\sqrt{4\varphi zx}\right).\end{aligned} \tag{44}$$

The proof of Lemma 2 is complete.

APPENDIX C
PROOF OF PROPOSITION 2

From (10), we have CDF of $F_{\gamma_{U_1}^{x_1}}$ is given by

$$\begin{aligned}F_{\gamma_{U_1}^{x_1}}(x)=1&-\sqrt{\upsilon_2x}K_1\left(\sqrt{\upsilon_2x}\right)-\sqrt{\upsilon_1x}K_1\left(\sqrt{\upsilon_1x}\right)\\&+\sqrt{\upsilon_3x}K_1\left(\sqrt{\upsilon_3x}\right),\end{aligned} \tag{45}$$

where $\upsilon_1=\frac{4d_0^\alpha d_1^\alpha}{\rho_S b_1\lambda_{h_0}\lambda_{\bar{h}_1}}$, $\upsilon_2=\frac{4d_0^\alpha d_1^\alpha}{\rho_S b_1\lambda_{h_0}\lambda_{\bar{h}_2}}$ and $\upsilon_3=\frac{4\varphi d_0^\alpha d_1^\alpha}{\rho_S b_1}$.

Next, the average BLER analysis of U_1 in the HRIS-assisted downlink NOMA system is given by

$$\begin{aligned}\tilde{\varepsilon}_{U_1}&=g_{U_1}\sqrt{\mathcal{L}_{U_1}}\int_{\alpha_{U_1}}^{\beta_{U_1}}F_{\gamma_{U_1}^{x_1}}(x)dx\\&=1-g_{U_1}\sqrt{\mathcal{L}_{U_1}}\\&\quad\times\left[I\left(\upsilon_2,x\right)+I\left(\upsilon_1,x\right)-I\left(\upsilon_3,x\right)\right],,\end{aligned} \tag{46}$$

Here $I(a,x)=\int_{\alpha_{U_1}}^{\beta_{U_1}}\sqrt{ax}K_1\left(\sqrt{ax}\right)dx$.

According to (46), $I(a,x)$ is obtained as follows

$$\begin{aligned}I(a,x)&=\int_{\alpha_{U_1}}^{\beta_{U_1}}\sqrt{ax}K_1\left(\sqrt{ax}\right)dx\\&=\int_0^\infty H\left(\left|\frac{x}{\alpha_{U_1}}\right|-1\right)H\left(1-\left|\frac{x}{\beta_{U_1}}\right|\right)\\&\quad\times\sqrt{ax}K_1\left(\sqrt{ax}\right)dx,\end{aligned} \tag{47}$$

where $H(x)$ denotes the Heaviside step function.

To solve the integrals (47), we utilize the following transformations involving the Meijer G-function [58, Chpt. 8.4]:

$$H(1-|x|)=G_{1,1}^{1,0}\left(x\,\middle|\,\begin{matrix}1\\0\end{matrix}\right), \tag{48}$$

$$H(|x|-1)=G_{1,1}^{0,1}\left(x\,\middle|\,\begin{matrix}1\\0\end{matrix}\right), \tag{49}$$

$$K_v(x)x^\mu=2^{\mu-1}G_{0,2}^{2,0}\left(\frac{x^2}{4}\,\middle|\,\begin{matrix}-\\\frac{1}{2}(\mu+v),\frac{1}{2}(\mu-v)\end{matrix}\right), \tag{50}$$

$$\int_0^\infty x^{\lambda-1} G_{p,q}^{m,0}\left(\eta x \middle| \begin{matrix}\mathbf{a}_p\\ \mathbf{b}_q\end{matrix}\right) G_{p_2,q_2}^{m_2,n_2}\left(\theta x^h \middle| \begin{matrix}\mathbf{c}_{p_2}\\ \mathbf{d}_{q_2}\end{matrix}\right) G_{p_3,q_3}^{m_3,n_3}\left(\delta x^k \middle| \begin{matrix}\mathbf{e}_{p_3}\\ \mathbf{f}_{q_3}\end{matrix}\right) dx = \eta^{-\lambda} \times \mathcal{H}_{q,p:p_2,q_2:p_3,q_3}^{0,m:m_2,n_2:m_3,n_3}\left(\begin{matrix}(1-\mathbf{b}_q-\lambda; h,k)\\ (1-\mathbf{a}_p-\lambda; h,k)\end{matrix} \middle| \begin{matrix}(\mathbf{c}_{p_2},1)\\ (\mathbf{d}_{q_2},1)\end{matrix} \middle| \begin{matrix}(\mathbf{e}_{p_3},1)\\ (\mathbf{f}_{q_3},1)\end{matrix} \middle| \frac{\theta}{\eta^h}, \frac{\delta}{\eta^k}\right). \tag{51}$$

$$\begin{aligned} I(a,x) &= \int_0^\infty G_{0,2}^{2,0}\left(\frac{a}{4}x \middle| \begin{matrix}-\\ 1,0\end{matrix}\right) G_{1,1}^{1,0}\left(\frac{1}{\beta_{U_1}}x \middle| \begin{matrix}1\\ 0\end{matrix}\right) G_{1,1}^{0,1}\left(\frac{1}{\alpha_{U_1}}x \middle| \begin{matrix}1\\ 0\end{matrix}\right) dx \\ &= \left(\frac{4}{a}\right) H_{2,0:1,1:1,1}^{0,2:1,0:0,1}\left(\begin{matrix}(-1;1,1);(0;1,1)\\ -\end{matrix} \middle| \begin{matrix}(1,1)\\ (0,1)\end{matrix} \middle| \begin{matrix}(1,1)\\ (0,1)\end{matrix} \middle| \frac{4}{a\beta_{U_1}}, \frac{4}{a\alpha_{U_1}}\right) \end{aligned} \tag{52}$$

and the following connection established by using the identity [57, Eq. (2.3)] and the connection [58, Eq. (8.3.2.21)] is displayed on the next page.

In (51), as shown at the top of the page, $\mathcal{H}_{p,q:u,v:e,f}^{m,n:s,t:i,j}(\cdot)$ stands for the extended generalized bivariate Fox H-function (EGBFHF) [57]. This function is easily assessed with mathematical tools such as Mathematica [59] and Matlab [60].

Substituting (50), (49) and (48) into (47) and using (51) $I(a,x)$ is given by (52), as shown at the top of the page.

Substituting (52) into (46), we can obtain (15).

The proof of Proposition 2 is completed.

APPENDIX D
PROOF OF PROPOSITION 3

Form (9), the CDF of $F_{\gamma_{U_2}^{x_2}}$ is given by

$$F_{\gamma_{U_2}^{x_2}}(z) = 1 - \sqrt{\frac{4\varphi d_0^\alpha d_2^\alpha z}{\rho_S(b_2-b_1 z)}} K_1\left(\sqrt{\frac{4\varphi d_0^\alpha d_2^\alpha z}{\rho_S(b_2-b_1 z)}}\right). \tag{53}$$

The analytical formulations of the effective capacities U_2 are provided by

$$\begin{aligned} \tilde{\varepsilon}_{U_2} &= g_{U_2}\sqrt{\mathcal{L}_{U_2}} \int_{\alpha_{U_2}}^{\beta_{U_2}} F_{\gamma_{U_2}^{x_2}}(x) dx \\ &= 1 - g_{U_2}\sqrt{\mathcal{L}_{U_2}} \int_{\alpha_{U_2}}^{\beta_{U_2}} \sqrt{4\varphi\hat{\theta}_2(x)} K_1\left(\sqrt{4\varphi\hat{\theta}_2(x)}\right) dx, \end{aligned} \tag{54}$$

where $\hat{\theta}_2(x) = \frac{d_0^\alpha d_2^\alpha x}{\rho_S(b_2-b_1 x)}$.

The integral (54) is first solved by expressing the Besselk function with the Meijer G-function using (50), and $\tilde{\varepsilon}_{U_2}$ is obtained as

$$\tilde{\varepsilon}_{U_2} = 1 - g_{U_2}\sqrt{\mathcal{L}_{U_2}} \int_{\alpha_{U_2}}^{\beta_{U_2}} G_{0,2}^{2,0}\left(\varphi\hat{\theta}_2(x) \middle| \begin{matrix}-\\ 1,0\end{matrix}\right) dx. \tag{55}$$

Though obtaining a closed-form formula for (55) is challenging, we can acquire an accurate approximation for it. We have used the Gaussian-Chebyshev quadrature [61, Eq. (25.4.38)], we have

$$\begin{aligned} &\int_a^b F(x)\,dx = \int_{-1}^1 F\left(y\left(\tfrac{b-a}{2}\right) + \left(\tfrac{a+b}{2}\right)\right)\tfrac{b-a}{2} dy \\ &\approx \tfrac{b-a}{2}\tfrac{\pi}{N}\sum_{n=1}^N \sqrt{1-\upsilon_w^2} F\left(\upsilon_w\left(\tfrac{b-a}{2}\right) + \left(\tfrac{a+b}{2}\right)\right) \end{aligned}, b < \infty \tag{56}$$

Substituting (56) into (55), we can obtain an approximation of (17)

The proof of Proposition 3 is completed.

REFERENCES

[1] Y. Chen, N. Zhang, Y. Zhang, and X. Chen, "Dynamic computation offloading in edge computing for Internet of Things," *IEEE Internet Things J.*, vol. 6, no. 3, pp. 4242–4251, Jun. 2019.

[2] L. Xu, J. Wang, X. Li, F. Cai, Y. Tao, and T. A. Gulliver, "Performance analysis and prediction for mobile Internet-of-Things (IoT) networks: A CNN approach," *IEEE Internet Things J.*, vol. 8, no. 17, pp. 13355–13366, Sep. 2021.

[3] A.-T. Le, D.-H. Tran, C.-B. Le, P. T. Tin, T. N. Nguyen, Z. Ding, H. V. Poor, and M. Voznak, "Power beacon and NOMA-assisted cooperative IoT networks with co-channel interference: Performance analysis and deep learning evaluation," *IEEE Trans. Mobile Comput.*, early access, Nov. 17, 2024, doi: 10.1109/TMC.2023.3333764.

[4] S. Jacob, V. G. Menon, S. Joseph, P. G. Vinoj, A. Jolfaei, J. Lukose, and G. Raja, "A novel spectrum sharing scheme using dynamic long short-term memory with CP-OFDMA in 5G networks," *IEEE Trans. Cognit. Commun. Netw.*, vol. 6, no. 3, pp. 926–934, Sep. 2020.

[5] Y. Huo, X. Dong, W. Xu, and M. Yuen, "Enabling multi-functional 5G and beyond user equipment: A survey and tutorial," *IEEE Access*, vol. 7, pp. 116975–117008, 2019.

[6] C. Huang, A. Zappone, G. C. Alexandropoulos, M. Debbah, and C. Yuen, "Reconfigurable intelligent surfaces for energy efficiency in wireless communication," *IEEE Trans. Wireless Commun.*, vol. 18, no. 8, pp. 4157–4170, Aug. 2019.

[7] T.-H. Vu, T.-V. Nguyen, D. B. D. Costa, and S. Kim, "Reconfigurable intelligent surface-aided cognitive NOMA networks: Performance analysis and deep learning evaluation," *IEEE Trans. Wireless Commun.*, vol. 21, no. 12, pp. 10662–10677, Dec. 2022.

[8] A.-T. Le, T. N. Nguyen, L.-T. Tu, T.-P. Tran, T. T. Duy, M. Voznak, and Z. Ding, "Performance analysis of RIS-assisted ambient backscatter communication systems," *IEEE Wireless Commun. Lett.*, vol. 13, no. 3, pp. 791–795, Mar. 2024.

[9] R. Deng, B. Di, H. Zhang, Y. Tan, and L. Song, "Reconfigurable holographic surface: Holographic beamforming for metasurface-aided wireless communications," *IEEE Trans. Veh. Technol.*, vol. 70, no. 6, pp. 6255–6259, Jun. 2021.

[10] C. Huang, S. Hu, G. C. Alexandropoulos, A. Zappone, C. Yuen, R. Zhang, M. D. Renzo, and M. Debbah, "Holographic MIMO surfaces for 6G wireless networks: Opportunities, challenges, and trends," *IEEE Wireless Commun.*, vol. 27, no. 5, pp. 118–125, Oct. 2020.

[11] Y. Ma, X. Shao, and W. Luo, "Holographic reconfigurable intelligent surface based on Holl effect for electromagnetic recording," in *Proc. Photon. Electromagn. Res. Symp. (PIERS)*, Nov. 2021, pp. 184–187.

[12] C. Yue, V. Miloslavskaya, M. Shirvanimoghaddam, B. Vucetic, and Y. Li, "Efficient decoders for short block length codes in 6G URLLC," *IEEE Commun. Mag.*, vol. 61, no. 4, pp. 84–90, Apr. 2023.

[13] P. Schulz, M. Matthe, H. Klessig, M. Simsek, G. Fettweis, J. Ansari, S. A. Ashraf, B. Almeroth, J. Voigt, I. Riedel, A. Puschmann, A. Mitschele-Thiel, M. Müller, T. Elste, and M. Windisch, "Latency critical IoT applications in 5G: Perspective on the design of radio interface and network architecture," *IEEE Commun. Mag.*, vol. 55, no. 2, pp. 70–78, Feb. 2017.

[14] L. Chettri and R. Bera, "A comprehensive survey on Internet of Things (IoT) toward 5G wireless systems," *IEEE Internet Things J.*, vol. 7, no. 1, pp. 16–32, Jan. 2020.

[15] G. Durisi, T. Koch, and P. Popovski, "Toward massive, ultrareliable, and low-latency wireless communication with short packets," *Proc. IEEE*, vol. 104, no. 9, pp. 1711–1726, Sep. 2016.

[16] Y. Polyanskiy, H. V. Poor, and S. Verdu, "Channel coding rate in the finite blocklength regime," *IEEE Trans. Inf. Theory*, vol. 56, no. 5, pp. 2307–2359, May 2010.

[17] P. Popovski, J. J. Nielsen, C. Stefanovic, E. D. Carvalho, E. Strom, K. F. Trillingsgaard, A.-S. Bana, D. M. Kim, R. Kotaba, J. Park, and R. B. Sorensen, "Wireless access for ultra-reliable low-latency communication: Principles and building blocks," *IEEE Netw.*, vol. 32, no. 2, pp. 16–23, Mar. 2018.

[18] M. Shirvanimoghaddam, M. S. Mohammadi, R. Abbas, A. Minja, C. Yue, B. Matuz, G. Han, Z. Lin, W. Liu, Y. Li, S. Johnson, and B. Vucetic, "Short block-length codes for ultra-reliable low latency communications," *IEEE Commun. Mag.*, vol. 57, no. 2, pp. 130–137, Feb. 2019.

[19] T.-H. Vu, T.-V. Nguyen, T.-T. Nguyen, V. N. Q. Bao, and S. Kim, "Short-packet communications in NOMA-CDRT IoT networks with cochannel interference and imperfect SIC," *IEEE Trans. Veh. Technol.*, vol. 71, no. 5, pp. 5552–5557, May 2022.

[20] Z. Ding, Y. Liu, J. Choi, Q. Sun, M. Elkashlan, I. Chih-Lin, and H. V. Poor, "Application of non-orthogonal multiple access in LTE and 5G networks," *IEEE Commun. Mag.*, vol. 55, no. 2, pp. 185–191, Feb. 2017.

[21] D.-T. Do, A.-T. Le, and B. M. Lee, "NOMA in cooperative underlay cognitive radio networks under imperfect SIC," *IEEE Access*, vol. 8, pp. 86180–86195, 2020.

[22] D.-T. Do, A.-T. Le, Y. Liu, and A. Jamalipour, "User grouping and energy harvesting in UAV-NOMA system with AF/DF relaying," *IEEE Trans. Veh. Technol.*, vol. 70, no. 11, pp. 11855–11868, Nov. 2021.

[23] L. Dai, B. Wang, Z. Ding, Z. Wang, S. Chen, and L. Hanzo, "A survey of non-orthogonal multiple access for 5G," *IEEE Commun. Surveys Tuts.*, vol. 20, no. 3, pp. 2294–2323, 3rd Quart., 2018.

[24] Y. Liu, Z. Qin, M. Elkashlan, Z. Ding, A. Nallanathan, and L. Hanzo, "Nonorthogonal multiple access for 5G and beyond," *Proc. IEEE*, vol. 105, no. 12, pp. 2347–2381, Dec. 2017.

[25] M. Shirvanimoghaddam, M. Dohler, and S. J. Johnson, "Massive non-orthogonal multiple access for cellular IoT: Potentials and limitations," *IEEE Commun. Mag.*, vol. 55, no. 9, pp. 55–61, Sep. 2017.

[26] G. Yang, X. Xu, and Y.-C. Liang, "Intelligent reflecting surface assisted non-orthogonal multiple access," in *Proc. IEEE Wireless Commun. Netw. Conf. (WCNC)*, May 2020, pp. 1–6.

[27] Z. Ding, R. Schober, and H. V. Poor, "On the impact of phase shifting designs on IRS-NOMA," *IEEE Wireless Commun. Lett.*, vol. 9, no. 10, pp. 1596–1600, Oct. 2020.

[28] X. Mu, Y. Liu, L. Guo, J. Lin, and N. Al-Dhahir, "Exploiting intelligent reflecting surfaces in NOMA networks: Joint beamforming optimization," *IEEE Trans. Wireless Commun.*, vol. 19, no. 10, pp. 6884–6898, Oct. 2020.

[29] M. Elhattab, M.-A. Arfaoui, C. Assi, and A. Ghrayeb, "Reconfigurable intelligent surface assisted coordinated multipoint in downlink NOMA networks," *IEEE Commun. Lett.*, vol. 25, no. 2, pp. 632–636, Feb. 2021.

[30] T. Hou, Y. Liu, Z. Song, X. Sun, Y. Chen, and L. Hanzo, "Reconfigurable intelligent surface aided NOMA networks," *IEEE J. Sel. Areas Commun.*, vol. 38, no. 11, pp. 2575–2588, Nov. 2020.

[31] C. Zhang, W. Yi, Y. Liu, and Q. Wang, "Multi-cell NOMA: Coherent reconfigurable intelligent surfaces model with stochastic geometry," in *Proc. ICC IEEE Int. Conf. Commun.*, Jun. 2021, pp. 1–6.

[32] Z. Ding and H. V. Poor, "A simple design of IRS-NOMA transmission," *IEEE Commun. Lett.*, vol. 24, no. 5, pp. 1119–1123, May 2020.

[33] X. Yue and Y. Liu, "Performance analysis of intelligent reflecting surface assisted NOMA networks," *IEEE Trans. Wireless Commun.*, vol. 21, no. 4, pp. 2623–2636, Apr. 2022.

[34] R. Hashemi, S. Ali, N. H. Mahmood, and M. Latva-Aho, "Average rate and error probability analysis in short packet communications over RIS-aided URLLC systems," *IEEE Trans. Veh. Technol.*, vol. 70, no. 10, pp. 10320–10334, Oct. 2021.

[35] H. Ren, K. Wang, and C. Pan, "Intelligent reflecting surface-aided URLLC in a factory automation scenario," *IEEE Trans. Commun.*, vol. 70, no. 1, pp. 707–723, Jan. 2022.

[36] A. Ranjha and G. Kaddoum, "URLLC facilitated by mobile UAV relay and RIS: A joint design of passive beamforming, blocklength, and UAV positioning," *IEEE Internet Things J.*, vol. 8, no. 6, pp. 4618–4627, Mar. 2021.

[37] Z. Zheng, L. Yuan, and F. Fang, "Performance analysis of fountain coded non-orthogonal multiple access with finite blocklength," *IEEE Wireless Commun. Lett.*, vol. 10, no. 8, pp. 1752–1756, Aug. 2021.

[38] T.-H. Vu, T.-V. Nguyen, D. B. D. Costa, and S. Kim, "Intelligent reflecting surface-aided short-packet non-orthogonal multiple access systems," *IEEE Trans. Veh. Technol.*, vol. 71, no. 4, pp. 4500–4505, Apr. 2022.

[39] A.-T. Le, N. X. Ha, D.-T. Do, A. Silva, and S. Yadav, "Enabling user grouping and fixed power allocation scheme for reconfigurable intelligent surfaces-aided wireless systems," *IEEE Access*, vol. 9, pp. 92263–92275, 2021.

[40] C.-B. Le, D.-T. Do, X. Li, Y.-F. Huang, H.-C. Chen, and M. Voznak, "Enabling NOMA in backscatter reconfigurable intelligent surfaces-aided systems," *IEEE Access*, vol. 9, pp. 33782–33795, 2021.

[41] A. P. Chrysologou, A. A. Boulogeorgos, N. D. Chatzidiamantis, and A. Alexiou, "Outage analysis of holographic surface assisted downlink terahertz NOMA," in *Proc. GLOBECOM IEEE Global Commun. Conf.*, Dec. 2022, pp. 5249–5254.

[42] A. P. Chrysologou, A.-A. A. Boulogeorgos, and N. D. Chatzidiamantis, "When THz-NOMA meets holographic reconfigurable intelligent surfaces," *IEEE Communications Letters*, vol. 27, no. 9, pp. 2516–2520, Jul. 2023.

[43] S. Q. Nguyen, A.-T. Le, C.-B. Le, P. T. Tin, and Y.-H. Kim, "Exploiting user clustering and fixed power allocation for multi-antenna UAV-assisted IoT systems," *Sensors*, vol. 23, no. 12, p. 5537, Jun. 2023. [Online]. Available: https://www.mdpi.com/1424-8220/23/12/5537

[44] T.-T.-T. Nguyen and X.-X. Nguyen, "Average block error rate analysis of IRS-aided NOMA short-packet communication systems," in *Proc. Int. Symp. Electr. Electron. Eng. (ISEE)*, Oct. 2023, pp. 91–96.

[45] T.-H. Vu, T.-T. Nguyen, Q.-V. Pham, D. B. da Costa, and S. Kim, "A novel partial decode-and-amplify NOMA-inspired relaying protocol for uplink short-packet communications," *IEEE Wireless Commun. Lett.*, vol. 12, no. 7, pp. 1244–1248, Jul. 2023.

[46] K. Guo, R. Liu, X. Li, L. Yang, K. An, and Y. Huang, "Outage performance of RIS-assisted cognitive non-terrestrial network with NOMA," *IEEE Trans. Veh. Technol.*, vol. 73, no. 4, pp. 5953–5958, Apr. 2024.

[47] T. N. Do, G. Kaddoum, T. L. Nguyen, D. B. da Costa, and Z. J. Haas, "Multi-RIS-aided wireless systems: Statistical characterization and performance analysis," *IEEE Trans. Commun.*, vol. 69, no. 12, pp. 8641–8658, Dec. 2021.

[48] R. Deng, B. Di, H. Zhang, D. Niyato, Z. Han, H. V. Poor, and L. Song, "Reconfigurable holographic surfaces for future wireless communications," *IEEE Wireless Commun.*, vol. 28, no. 6, pp. 126–131, Dec. 2021.

[49] R. Deng, B. Di, H. Zhang, Y. Tan, and L. Song, "Reconfigurable holographic surface-enabled multi-user wireless communications: Amplitude-controlled holographic beamforming," *IEEE Trans. Wireless Commun.*, vol. 21, no. 8, pp. 6003–6017, Aug. 2022.

[50] D.-T. Do, M.-S. Van Nguyen, M. Voznak, A. Kwasinski, and J. N. de Souza, "Performance analysis of clustering car-following V2X system with wireless power transfer and massive connections," *IEEE Internet Things J.*, vol. 9, no. 16, pp. 14610–14628, Aug. 2022.

[51] T. T. Phu, T. H. Dang, T. D. Tran, and M. Voznak, "Security-reliability analysis of noma-based multi-hop relay networks in presence of an active eavesdropper with imperfect eavesdropping CSI," *Adv. Electr. Electron. Eng.*, vol. 15, no. 4, pp. 591–597, Nov. 2017.
[52] T.-N. Tran, D.-T. Do, and M. Voznak, "On outage probability and throughput performance of cognitive radio inspired NOMA relay system," *Adv. Electr. Electron. Eng.*, vol. 16, no. 4, pp. 501–512, Dec. 2018.
[53] A. A. Boulogeorgos, N. D. Chatzidiamantis, H. G. Sandalidis, A. Alexiou, and M. D. Renzo, "Cascaded composite turbulence and misalignment: Statistical characterization and applications to reconfigurable intelligent surface-empowered wireless systems," *IEEE Trans. Veh. Technol.*, vol. 71, no. 4, pp. 3821–3836, Apr. 2022.
[54] V. D. Phan, T. L. Nguyen, T. T. Phu, and V. V. Nguyen, "Reliability-security in wireless-powered cooperative network with friendly jammer," *Adv. Electr. Electron. Eng.*, vol. 20, no. 4, pp. 584–591, Feb. 2023.
[55] I. S. Gradshteyn and I. M. Ryzhik, *Table of Integrals, Series, and Products*. New York, NY, USA: Academic, 2014.
[56] N. Agrawal, A. Bansal, K. Singh, C.-P. Li, and S. Mumtaz, "Finite block length analysis of RIS-assisted UAV-based multiuser IoT communication system with non-linear EH," *IEEE Trans. Commun.*, vol. 70, no. 5, pp. 3542–3557, May 2022.
[57] P. K. Mittal and K. C. Gupta, "An integral involving generalized function of two variables," *Proc. Indian Acad. Sci. Sect. A*, vol. 75, no. 3, pp. 117–123, Mar. 1972. [Online]. Available: https://api.semanticscholar.org/CorpusID:117253163
[58] A. Prodnikov, Y. A. Brychkov, and O. Marichev, *Integrals and Series. Volume 3, More Special Functions*, vol. 3. London, U.K.: Gordon and Breach Science, 1986.
[59] H. Lei, I. S. Ansari, G. Pan, B. Alomair, and M.-S. Alouini, "Secrecy capacity analysis over $\alpha-\mu$ fading channels," *IEEE Commun. Lett.*, vol. 21, no. 6, pp. 1445–1448, Jun. 2017.
[60] K. P. Peppas, "A new formula for the average bit error probability of dual-hop amplify-and-forward relaying systems over generalized shadowed fading channels," *IEEE Wireless Commun. Lett.*, vol. 1, no. 2, pp. 85–88, Apr. 2012.
[61] M. Abramowitz, I. A. Stegun, and R. H. Romer, *Handbook of Mathematical Functions With Formulas, Graphs, and Mathematical Tables*, 1988.

DINH-TUNG VO received the Engineering degree in electrical and electronic engineering from the HCMC University of Technology and Education, Ho Chi Minh City, Vietnam, in 1998, the master's degree in control and automation engineering from Ho Chi Minh City University of Transport, Ho Chi Minh City, in 2008, and the Ph.D. degree in the system analysis, control system and data transfer from the Experimental Institute of Automotive Electronics and Electrical Equipment, the Ministry of Industry and Energy of the Russian Federation, Moscow, Russia.

TAN N. NGUYEN (Member, IEEE) was born in Nha Trang City, Vietnam, in 1986. He received the B.S. degree in electronics from Ho Chi Minh University of Natural Sciences, in 2008, the M.S. degree in telecommunications engineering from Vietnam National University, in 2012, and the Ph.D. degree in communications technologies from the Faculty of Electrical Engineering and Computer Science, VSB—Technical University of Ostrava, Czech Republic, in 2019. He joined the Faculty of Electrical and Electronics Engineering, Ton Duc Thang University, Vietnam, in 2013, and since then has been lecturing. His major research interests include cooperative communications, cognitive radio, signal processing, satellite communication, UAV, and physical layer security. He started as the Editor-in-Chief of *Advances in Electrical and Electronic Engineering* journal, in 2023.

ANH-TU LE (Member, IEEE) was born in Lam Dong, Vietnam, in 1997. He received the B.S. degree from the Industrial University of Ho Chi Minh City, Vietnam, in 2019, and the M.S. degree from Ton Duc Thang University, Vietnam, in 2022. He is currently pursuing the Ph.D. degree in communication technology with the VSB—Technical University of Ostrava, Czech Republic. He has authored or coauthored over 25 ISI-indexed journals. His research interests include wireless channel modeling, NOMA, cognitive radio, MIMO, and machine learning.

VAN-DUC PHAN was born in Long An, Vietnam, in 1975. He received the M.S. degree from the Department of Electrical, Electrical and Telecommunication Engineering, Ho Chi Minh City University of Transport, Ho Chi Minh City, Vietnam, and the Ph.D. degree from the Department of Mechanical and Automation Engineering, Da-Yeh University, Taiwan, in 2016. His current research interests include sliding mode control, non-linear systems or active magnetic bearing, flywheel store energy systems, power system optimization, optimization algorithms, renewable energies, energy harvesting (EH) enabled cooperative networks, improving the optical properties, lighting performance of white LEDs, energy efficiency LED driver integrated circuits, novel radio access technologies, and physical security in communication networks.

MIROSLAV VOZNAK (Senior Member, IEEE) received the Ph.D. degree in telecommunications from the Faculty of Electrical Engineering and Computer Science, VSB—Technical University of Ostrava, and the Habilitation degree, in 2009. He was appointed as a Full Professor in electronics and communications technologies, in 2017. He is currently a Principal Investigator in the Research Project QUANTUM5 funded by NATO, which focuses on the application of quantum cryptography in 5G campus networks. He participated in six projects funded by EU in programs managed directly by European Commission. He has authored or coauthored more than 100 articles in SCI/SCIE journals. His research interests include ICT, especially on quality of service and experience, network security, wireless networks, and big data analytics. According to the Stanford University study released, in 2020, he is one of the World's Top 2% of Scientists in networking and telecommunications, and information and communications technologies. He has served as the General Chair for the 11th IFIP Wireless and Mobile Networking Conference, in 2018, and the 24th IEEE/ACM International Symposium on Distributed Simulation and Real-Time Applications, in 2020.